Mechanical Quantification of Fibrosis in 2D & 3D Models using Atomic Force Microscopy

Placement Report
001050187

Author
Tarika Sodhi
Industrial Placement Student, GSK

Supervisor
Kirsty Ford
Principal Scientist, GSK

I spent my industrial placement year at GSK (GlaxoSmithKline), a global biopharmaceutical company known for its focus on innovative medicines and research across a range of therapeutic areas, including respiratory conditions, oncology and infectious diseases. Within GSK, I was part of the Respiratory Immunology Inflammation Biology Unit (RIIBU), a wonderful team dedicated to understanding the mechanisms that drive chronic respiratory diseases.

My project centred on idiopathic pulmonary fibrosis (IPF), a progressive and irreversible lung disease characterised by the abnormal build-up of extracellular matrix (ECM) proteins. This accumulation leads to increased tissue stiffness and significant loss of organ function[1]. Available treatments for IPF are limited and frequently associated with significant side effects. Because of this, developing new therapies to better target or slow fibrosis progression is a key priority for both GSK and IPF patients.

My project for the year was to quantify mechanical properties of fibrosis in 2D ECM models derived from IPF fibroblasts, using a novel technique and a new instrument called the Pavone Nanoindenter (Optics11 Life). This technology is based on atomic force microscopy and uses nanoscale indentation to measure mechanical properties like stiffness and viscoelasticity[2]. I was one of the first people at GSK to learn how to use this new device and played a key role in setting up and refining the protocols needed to build capability in this technology. Additionally, my project involved the development of 3D models of fibrosis utilizing IPF fibroblast spheroids. These are cell aggregates that mimic the architecture and mechanical environment of human tissue, providing a more physiologically relevant model for testing anti-fibrotic therapies than generic 2D ECM models.

This report provides an overview of the scientific background of IPF and explains why mechanical properties were selected as the focus of our study, followed by a description of the experimental design and execution using the 2D ECM model. I'll present key findings and discuss their implications, then outline the early work on setting up 3D spheroid models and their potential value in translational research. Finally, I'll reflect the next steps for the project beyond my placement and on the impact I was able to make during my time at GSK.

1. Introduction

Idiopathic pulmonary fibrosis (IPF) is a chronic and progressive lung condition with no known cause. Histologically, IPF is characterised by the presence of usual interstitial pneumonia (UIP), while clinically, it presents with unexplained chronic exertional dyspnoea (shortness of breath during physical activity), persistent dry cough, bibasilar inspiratory crackles on lung auscultation, and finger clubbing[3]. IPF is thought to result from repeated micro-injuries to the alveolar epithelium, which disrupt the normal wound healing process. Instead of resolution, these injuries lead to persistent fibroblast and myofibroblast activation and the overproduction of extracellular matrix (ECM) proteins such as collagen I and fibronectin[4].

One of the defining physical characteristics of IPF is increased tissue stiffness due to the build-up and cross-linking of ECM components, driven by enzymes like lysyl oxidase (LOX)[5]. However, matrix stiffening isn't just a by-product of fibrosis, it also contributes to the disease itself[6]. As stiffness increases, fibroblasts use mechanotransduction pathways to respond. These pathways usually involve integrins, focal adhesions, and downstream signals like RhoA/ROCK and YAP/TAZ[7]. These signals reinforce fibroblast activation and ECM production, creating a positive feedback loop that leads to sustained progressive fibrosis[8].

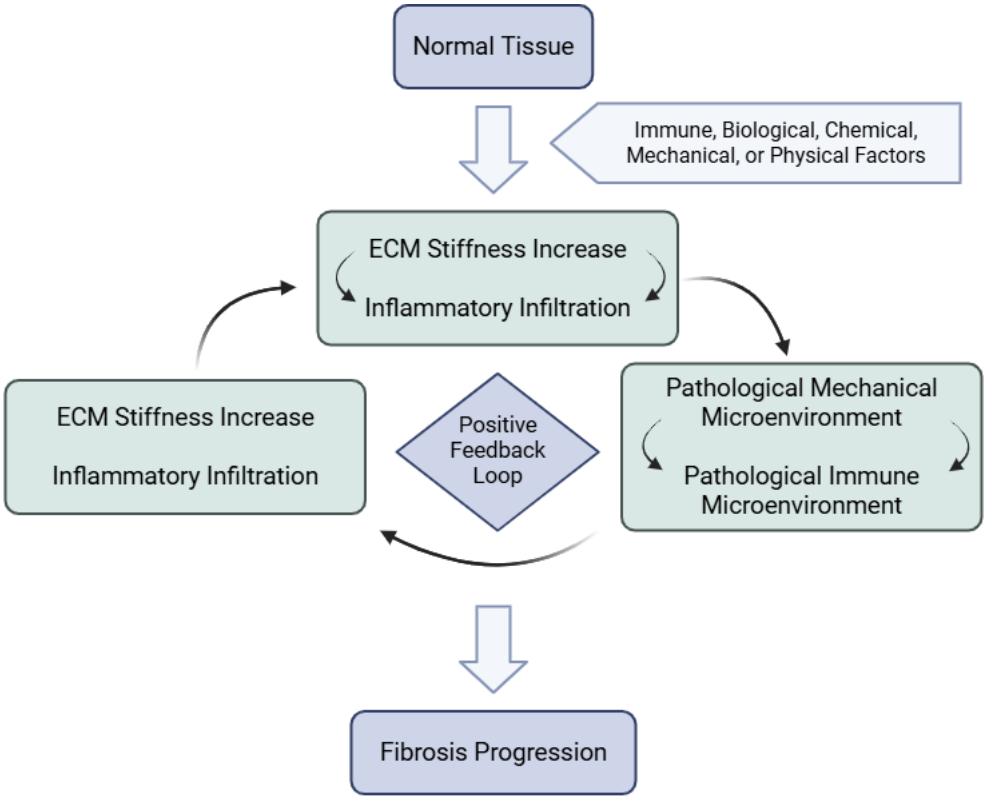

Figure 1: *Stiff ECM is more than a consequence of fibrosis—it becomes an active driver. In IPF, this creates a feedback loop that promotes fibroblast activation, ECM build-up, and impaired lung function. Created with Biorender.*

Because of this tight feedback between ECM stiffness and fibroblast behaviour, the mechanical properties of ECM could be an important readout of not only fibroblast pathology, but how this proceeds to impact lung tissue functionally; an important concept to explore with anti-fibrotic therapies[9]. In this project, the Pavone Nanoindenter by Optics11 Life, was used to quantify the stiffness and viscoelasticity of ECM derived from IPF fibroblasts to understand how fibroblasts alter the physical environment of the ECM.

A key part of this study involved comparing fibroblast production of ECM after pro-fibrotic treatment and perturbing this response with an experimental anti-fibrotic compound in development at GSK. This compound targets a key fibrotic cross-linking enzyme, referred to in this report as Target Enzyme (TE), which has been shown to be highly expressed in IPF patient lung tissue.

By comparing mechanical properties of ECM, this project aimed to understand the biophysical role of TE, moreover, if inhibiting it could restore stiffness and viscoelasticity driven by a pro-fibrotic environment. The Pavone Nanoindenter was central to this. It works by indenting a calibrated probe into a sample's surface and measuring how it deforms. From this, it extracts key mechanical values like Young's modulus and viscoelasticity[10].

What makes the Pavone stand out is its sensitivity and range. It can detect forces as low as 0.2 nanonewtons and as high as 1.5 millinewtons[11]. This means it can assess everything from ultra-soft hydrogels (10 Pa) to rigid biological samples (1 GPa). The system uses interchangeable probes, as seen

in Figure 2 (B), of varying stiffness and tip sizes, allowing for precise measurements across a wide range of samples—from as soft and fragile as healthy ECM to as stiff as tumour tissues!

The Pavone uses a cantilever-based sensing mechanism rooted in atomic force microscopy (AFM). Each probe vibrates at a known frequency. When the probe touches the sample, the cantilever bends depending on the material's resistance. This bending changes the probe's vibration, creating a phase shift relative to its base frequency. An optical fibre integrated into the probe as seen in Figure 2 (D) detects these shifts with nanometre-scale accuracy[12].

These phase shifts give real-time data on the force applied and how deep the probe indents. From this, Young's modulus can be calculated using standard contact mechanics models like the Hertz model[13]. Since the Pavone works under tightly controlled conditions, measurements of viscoelastic behaviour can also be explored by observing how ECM responds over time—not just in terms of stiffness, but also in how it stores and dissipates mechanical energy.

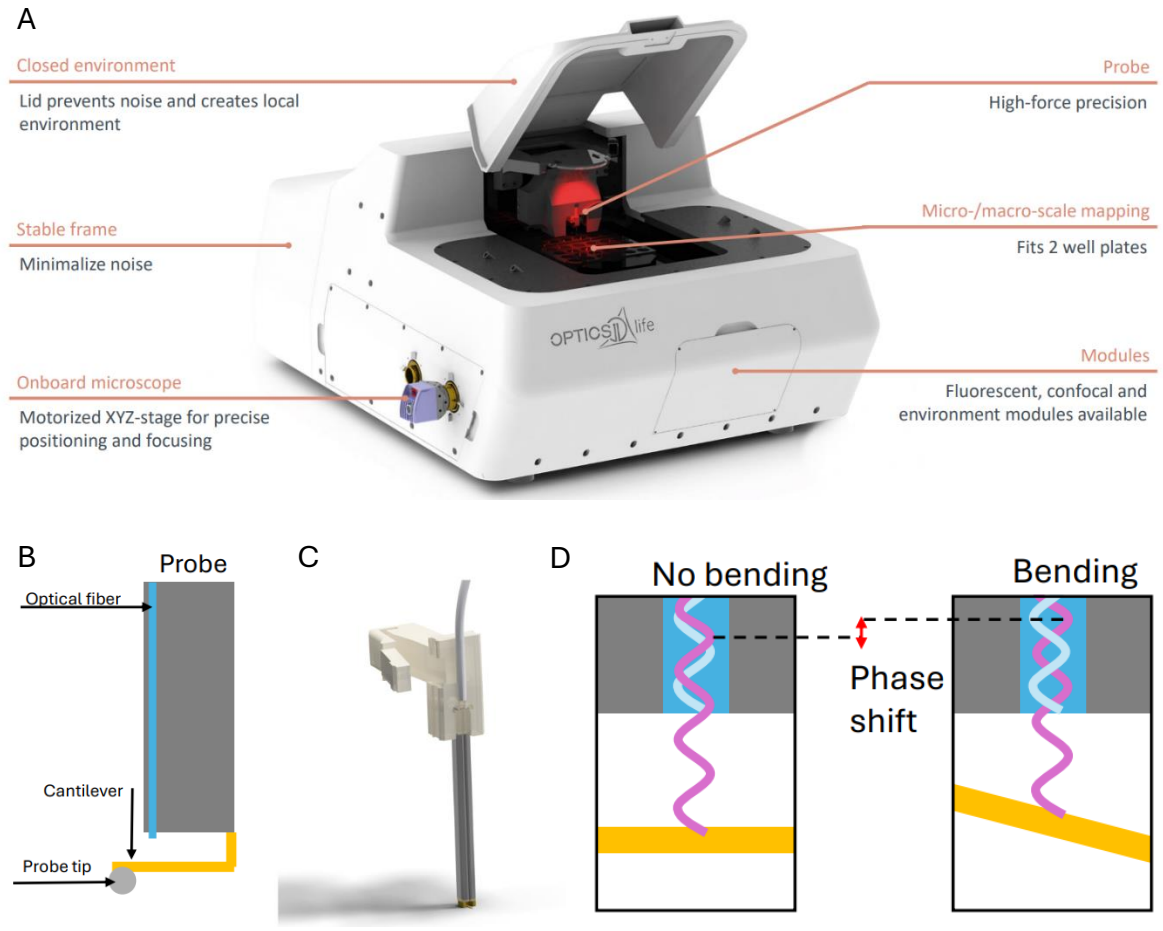

Figure 2: *(A) The Pavone system with its components labelled (B) Diagram of the probe, with labels indicating the tip, cantilever, and the optical fibre that measures cantilever movement during phase shift. (C) Image of the actual probe (D) Illustration of how the cantilever responds when it touches a sample: in air, it vibrates freely, but when it comes in contact with the surface causing it to bend, there is a phase shift in its oscillation, which is picked up by the optical fibre and used to calculate indentation depth.*[11]

Stiffness was quantified using Young's modulus (E), a standard mechanical property that describes a material's resistance to deformation[14]. It's calculated as the ratio of stress to strain, where stress is the applied force per unit area, and strain is the relative deformation of the material ($\Delta L/L_0$)[15]. In practice, a higher E value means the material is stiffer and deforms less under the same force, whereas a lower E indicates more flexibility[16].

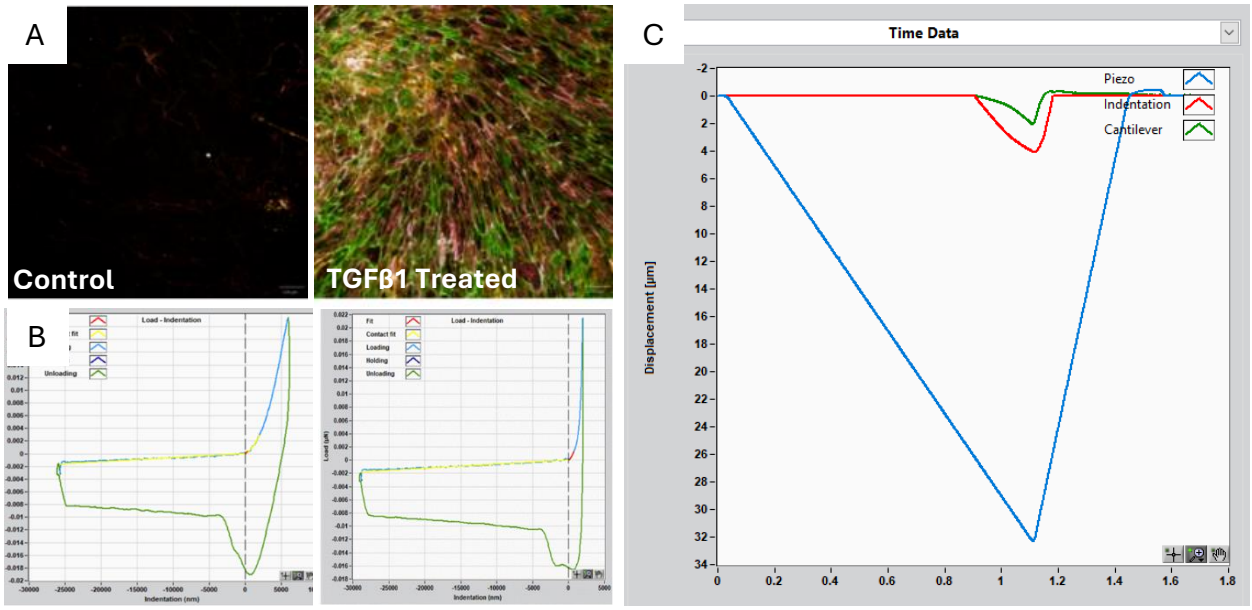

Figure 3: *(A) Immunofluorescence images (Operetta) showing less ECM in control wells and increased ECM deposition (collagen, fibronectin, TE) in TGF-β1-treated wells seeded with IPF fibroblasts. (B) Nanoindentation curves from Pavone.* ***Yellow:*** *Initial contact point (Hertz model fit).* ***Red:*** *Region used for stiffness calculation (overall fit).* ***Blue:*** *Loading phase as the indenter applies force.* ***Green:*** *Unloading phase (showing elastic recovery). (C) Probe trajectory during indentation showing approach, deformation of sample, and retraction from the ECM.*

Alongside stiffness, another critical mechanical property of ECM is its **viscoelasticity**, its combined solid-like and fluid-like response to deformation[17]. Biological tissues like lung ECM naturally show viscoelastic behaviour, which plays a key role in how cells sense and respond to their environment.

In fibrotic tissue, ECM becomes more tightly crosslinked, shifting it towards a more elastic (solid-like) state with reduced ability to dissipate energy. This increased viscoelasticity further contributes to abnormal cell behaviour and impairs normal lung mechanics[18]. That is why it's important to assess not only how stiff the ECM is, but also how its viscoelastic profile changes during fibrosis.

To measure this, we used **tan δ (delta)**, a value derived from oscillatory nanoindentation tests performed using the Pavone[19]. Tan δ is the ratio of the loss modulus (G″), which reflects viscous energy loss, to the storage modulus (G′), which reflects elastic energy storage:

tanδ=G″/G′

A lower tan δ indicates the ECM is behaving more like a rigid solid, typical of fibrotic tissue. A higher tan δ points to more fluid-like, dissipative behaviour, and is often a sign of healthier, more compliant ECM[20].

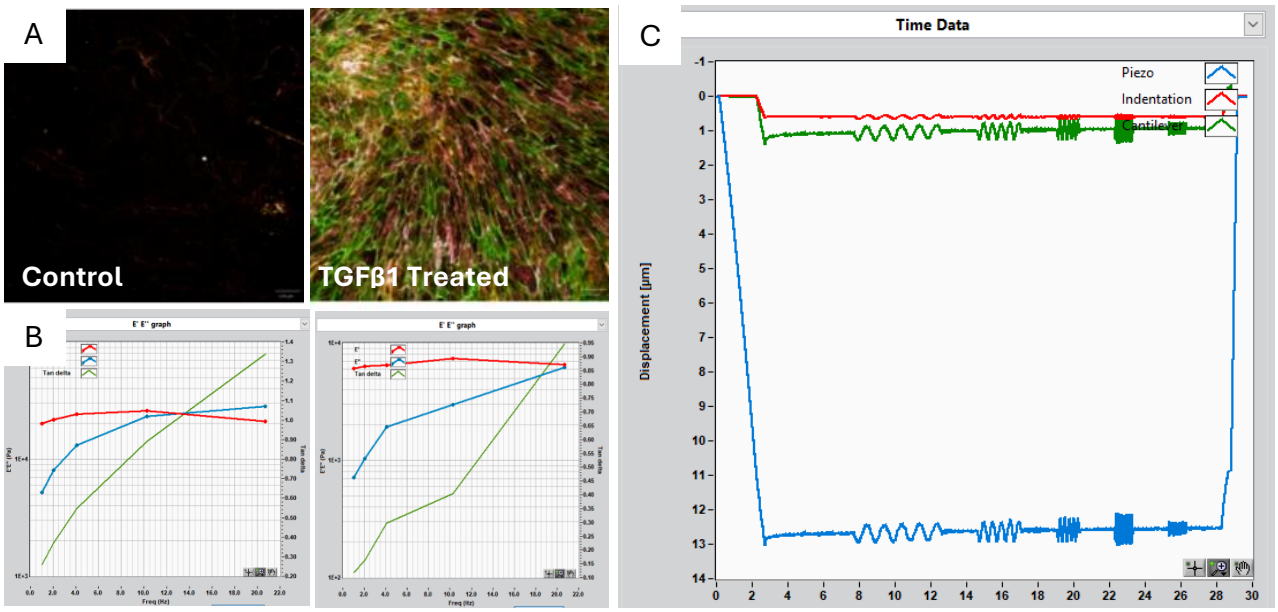

Figure 4: *(A) Immunofluorescence images (Operetta) showing less ECM in control wells and increased ECM deposition (collagen, fibronectin, TE) in TGF-β1-treated wells seeded with IPF fibroblasts. (B) Storage (E', elastic) and loss (E", viscous) modulus curves from indentation with Pavone, with the tan δ (E"/E') ratio plotted. A crossover between E' and E" indicates viscoelastic behaviour, while parallel curves indicate more elastic, solid-like ECM typical of fibrosis. (C) Probe trajectory showing indentation, oscillatory movements at various frequencies, and then retraction.*

By comparing Young's modulus and tan δ across treatment groups, this project aimed to determine whether targeting TE could help restore the mechanical balance of ECM produced by IPF fibroblasts.

2. Methods

2.1 IPF Fibroblast Cell Culture

IPF fibroblasts were cultured in high-serum DMEM under standard conditions (37°C, 5% CO_2) until they reached confluency. The cells were seeded into 96-well plates containing low-serum media and left to culture o/n for treatment the following day. For mechanical testing, treatments were applied in media formulations optimised to support ECM deposition and are detailed in section 2.2 below.

2.2 TGF-β1 Treatment of IPF Fibroblast ECM

To stimulate ECM synthesis and stiffening, cells were treated with 3 ng/mL TGF-β1 for six days. Control wells received the same assay media without TGF-β1. All cultures were maintained in low-serum conditions at 37°C and 5% CO_2 throughout the experiment. Some cells were left untreated to allow for a negative control in the experiment.

2.3 Combined TGF-β1 and TE Treatment

Cells were treated with either TGF-β1 (3 ng/mL), TE (500 µg/mL), or a combination of both. As before, treatments were administered in low-serum media, and cells were cultured under standard conditions (37°C, 5% CO_2) for six days.

2.4 TGF-β1 and TE Inhibitor Treatment Across Multiple Donors

To assess reproducibility, experiments were conducted using fibroblasts from three IPF donors. Cells were treated with 3uM of two TE inhibitors, either alone or in combination with TGF-β1. These were cultured in assay media and maintained at 37°C and 5% CO_2 for either three or six days, depending on the experimental set-up.

2.5 Decellularization and Fixation

Following treatment, ECM samples were decellularized using ammonium hydroxide and then fixed with cold methanol. After washing, the fixed ECM was stored in serum-containing media at 4°C until mechanical analysis.

2.6 Setting Up and Using the Pavone

Before use, the Pavone Nanoindenter was powered on by activating the interferometer, power supply, and PC, after checking all connections and releasing the stage lock. A soft probe (spring constant 0.019 N/m, 3 µm tip) was chosen to accommodate the delicate nature of the ECM samples, allowing for ~1 µm indentation depth. The probe was mounted and aligned in air using the onboard camera system. A 96-well plate layout was configured in the software for automated measurement.

Calibration was done in a clean well filled with the same medium as the samples. This involved entering probe parameters, running a wavelength scan, performing surface detection, and carrying out a three-step indentation to determine the probe's geometrical factor. Transit height and focal plane settings were adjusted to enable automated measurements across the plate.

To assess ECM stiffness, the experiment was configured to run displacement-controlled indentations first, to estimate appropriate load settings. For actual measurements, the "Peak Load Poking" mode was used. In this mode, the probe indents at a constant piezo speed until a set peak load is reached, then retracts—providing a balance between speed and accuracy for soft biological samples. A matrix scan (5×5 grid with 100 µm spacing) was defined for each selected well. Commands were programmed to centre the probe, find the surface, and apply a fixed peak load (e.g. 0.04 µN) at a controlled speed (30 µm/s). Stiffness data was extracted during post-processing using the Data Viewer software.

For viscoelastic characterisation, Dynamic Mechanical Analysis (DMA) was performed using the Pavone's oscillatory indentation mode. These experiments were set up using the instrument's "DMA" tab. Specific parameters were adjusted to ensure valid data: a 1-second relaxation time was included before oscillation to allow the sample to stabilise; an oscillation amplitude of 50 nm (10% of the 500 nm total indentation depth) was chosen to remain in the linear deformation range. Oscillations were carried out at multiple frequencies (1, 2, 4, 10, and 20 Hz), with each frequency receiving at least one full second of cyclic input. Measurements were taken in a low-noise environment to minimise

interference, and results were analysed using the built-in DMA analysis tools provided by Pavone's software.

2.7 Statistical Analysis

Mechanical data were exported from Data Viewer (Optics11 Life) and analysed using Spotfire and GraphPad. Where relevant, Kruskal–Wallis tests were applied to compare treatment conditions to the control group and assess statistical significance. Results were considered statistically significant when $p < 0.05$.

3. Results

3.1 Exploring Pro-Fibrotic and TE effects on ECM Stiffness

To evaluate how the exogenous addition of the Target Enzyme (TE) affects ECM stiffness, measurements were taken across four experimental conditions: untreated control, TGF-β1 treatment, TE-only, and TGF-β1 combined with TE. In addition, the influence of methanol fixation on ECM stiffness measurements was assessed using the Pavone Nanoindenter.

To account for variability in ECM thickness between groups, measurements were collected at two indentation depths: 250 nm and 750 nm. These values were selected based on the linear regions identified in the load–indentation curves. At 250 nm (Figure 5A), all samples could be measured. Control ECM showed a higher average Young's modulus than the ECM treated with TGF-β1. Further analysis of the curves revealed that, in TGF-β1-treated samples, the 250 nm indentation depth primarily captured surface resistance, rather than reflecting the full mechanical profile of the thicker ECM layer.

To overcome this limitation, the indentation depth was increased to 750 nm (Figure 5B), which better represented the mechanical behaviour of the denser matrix produced under TGF-β1 stimulation. At this greater depth, the probe made contact with the well plate in control samples due to their reduced ECM thickness, leading to poor curve fitting and N/A values. As a result, fewer successful indentations were obtained at 750 nm compared to 250 nm in the control samples.

Interestingly, the trend in stiffness reversed at the deeper indentation depth: TGF-β1 and TGF-β1 + TE-treated ECM showed higher stiffness than both the control and TE-only conditions. This pattern was observed only in methanol-fixed ECM. In unfixed samples, the ECM layer was generally too thin to allow reliable indentation at either depth, which resulted in mostly unmeasurable or excluded values.

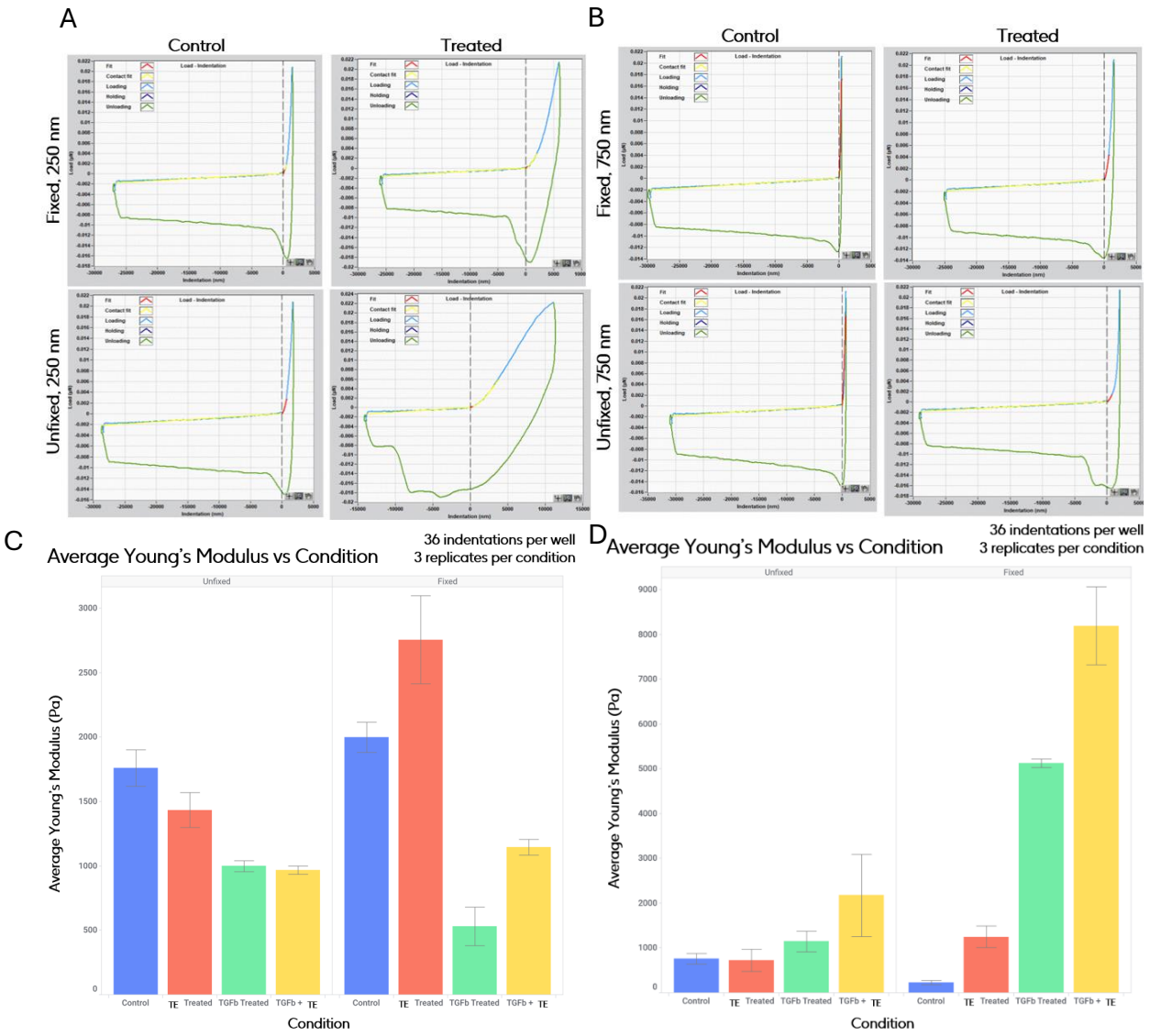

Figure 5. ***Load indentation curves and Young's modulus quantification for fixed and unfixed ECM under Control and TGF-β1 treated conditions at 250 nm and 750 nm indentations.*** *(A) Representative Load indentation curves at 250nm for control and TGF-β1 treated when fixed and unfixed. Red line = linear curve plotting hertz model by Pavone data viewer software from contact fit. (B) Representative Load indentation curves at 750nm for control and TGF-β1 treated when fixed and unfixed. Red line = linear curve plotting hertz model by Pavone data viewer software from contact fit. (C) Bar chart showing quantification of young's modulus (E) mean using Hertz equation at 250nm indentation depth for unfixed and fixed for untreated, TGF-β1 treated, TG2 treated, and combination. (D) Bar chart showing quantification of young's modulus (*E*) mean using Hertz equation at 750nm indentation depth for unfixed and fixed for untreated, TGF-β1 treated, TG2 treated, and combination. Data represents mean and Sd deviation, n=3 replicate wells per condition, n=36 indentations per well, n=1 donor.*

3.2 Measuring Young's Modulus in Multiple Donors

In figure 5 (B, D) we showed that TGFb1 enhanced ECM stiffness compared to control in fixed samples and that TE further enhanced this effect. We therefore wondered if the increased stiffness demonstrated with pro-fibrotic could be reduced with an inhibitor targeting TE. ECM stiffness was measured in three IPF fibroblast donors (L279, L287, and L300). Each donor's cells were treated with TGF-β1 alone or

in combination with TE inhibitors, and the resulting ECM was either fixed with methanol or left unfixed prior to testing.

The Pavone system was used to quantify stiffness, and results were expressed as average Young's modulus. As shown in Figure 6 (A–B), data were visualised in two ways: a scatter plot with individual replicate values, and a box plot showing donor-averaged results. Treatment groups are shown on the x-axis; stiffness in kilopascals is plotted on the y-axis.

Results varied between donors, but some trends can be observed in the fixed ECM samples. In donors L279 and L287, stiffness differed clearly between TGF-β1 and TE inhibitor conditions. These effects were specific to the fixed ECM, whilst in the unfixed samples, no difference in stiffness was observed between treatment groups. Of note, in the untreated control group due to ECM layers being too thin for accurate indentation, the Pavone returned very few data points, so the decision was taken to exclude this condition from the data.

When pooling stiffness data across all 3 donors as seen in Figures 6 (C–D), a statistically significant reduction in stiffness with TE Inhibitor A was observed in the fixed samples.

A

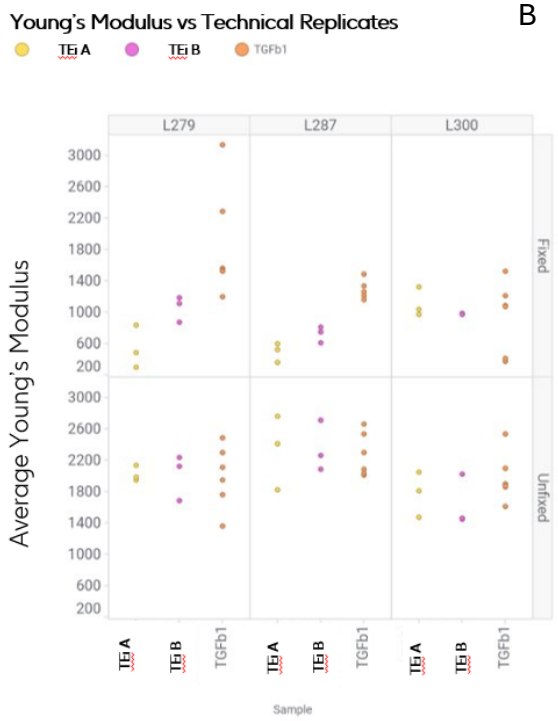

B

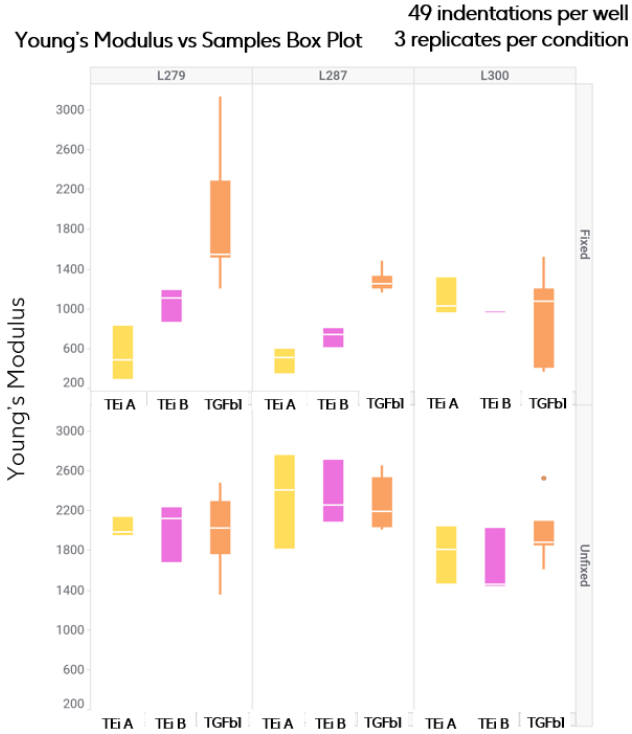

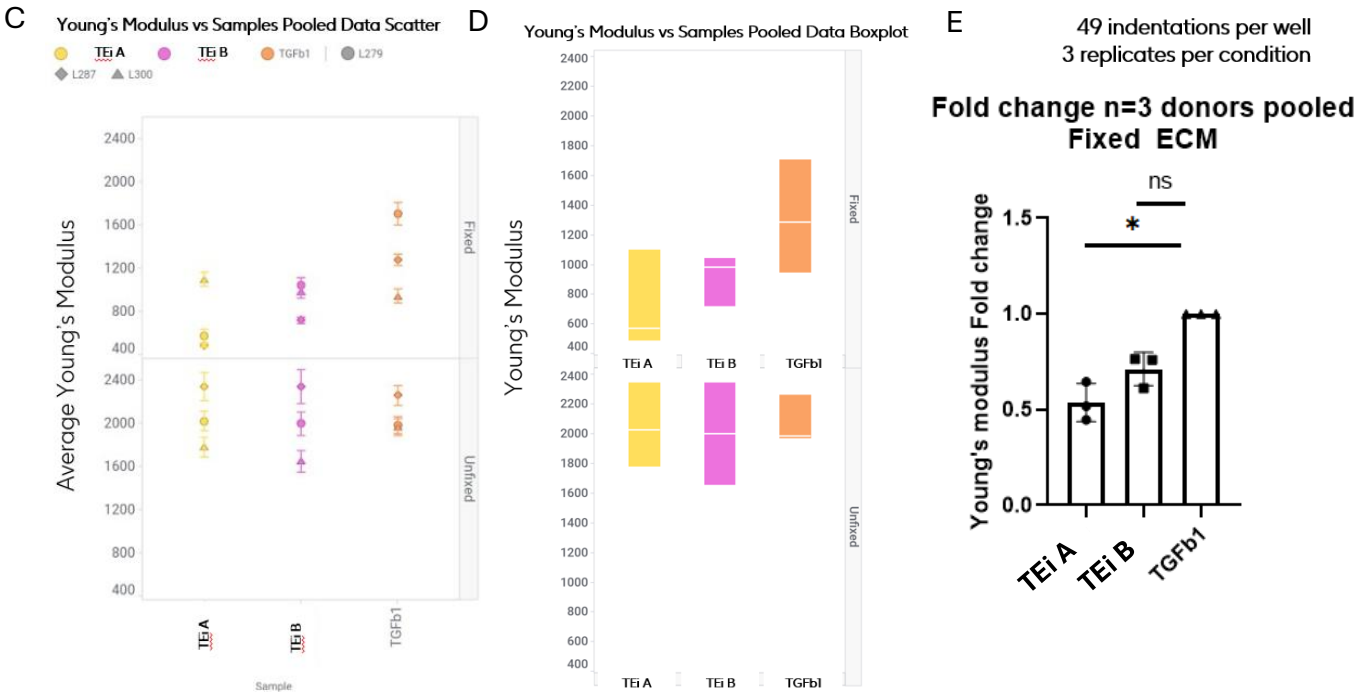

Figure 6. Quantification of ECM stiffness across fixed and unfixed conditions in multiple IPF fibroblast donors. *(A) Scatter plot showing individual replicate Young's modulus (kPa) measurements for fixed ECM from donors L279, L287, and L300 in fibroblasts treated with TGF-β1 +/- TEi A or B. (B) Box plot showing median and interquartile range of Young's modulus values across all donors for each condition. (C) Scatter plot showing mean of donor-averaged Young's modulus values grouped by fixation status. (D) Box plot showing median stiffness (kPa) per donor and condition. (E) Kruskal–Wallis fold change analysis results for fixed ECM across conditions. Control samples not shown due to low ECM yield. Data represents mean, median, and Sd deviation, n=3 replicate wells per condition, n=49 indentations per well, n=3 donor.*

3.3 Dynamic Measurement Analysis (DMA)

To explore how fibrosis affects the ECM's viscoelastic behaviour, dynamic mechanical analysis (DMA) was carried out on ECM treated with 3 ng/mL TGF-β1 and compared to untreated controls. Oscillations were applied at five different frequencies: 1, 2, 4, 10 and 20 Hz.

Across all frequencies, *tan δ* values were lower in the TGF-β1-treated ECM, suggesting a shift toward more elastic, solid-like mechanical behaviour, consistent with the idea that fibrosis leads to increased ECM crosslinking and reduced capacity for energy dissipation, a hallmark of stiffer, fibrotic matrix (Figure 7). Of note, unfixed samples could not be analysed for DMA due to their thin, fragile nature.

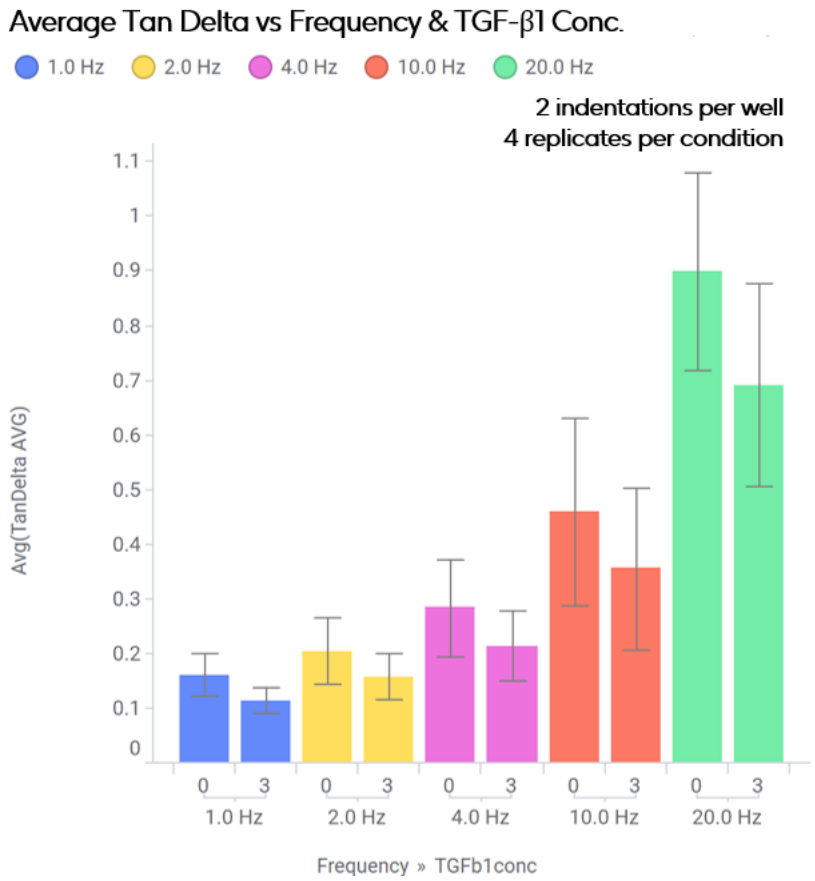

Figure 7. Bar plot showing average tan δ values across oscillation frequencies for untreated and TGF-β1-treated ECM. *Bar plot showing mean of average tan δ values (±SEM) recorded at 1, 2, 4, 10, and 20 Hz. Each condition includes four replicate measurements (two per well). Data represents mean and Sd deviation, n=4 replicate wells per condition n=1 donor.*

3.4 DMA: Effect of Fibrotic Stimuli, with/without TEi

In figure 7 we showed that TGFb1 reduced ECM viscoelasticity compared to control in fixed samples. Expanding on this we wanted to explore the effect of fibrotic stimuli and see if viscoelasticity could be altered in the presence of TE inhibitors. Moreover, to increase the robustness of the results, the number of replicates and indentations per well was increased.

The presence of the Target Enzyme inhibitor appeared to alter the tan δ values relative to TGF-β1 alone, reflecting a change in the ECM's viscoelastic behaviour under these conditions (Figure 8).

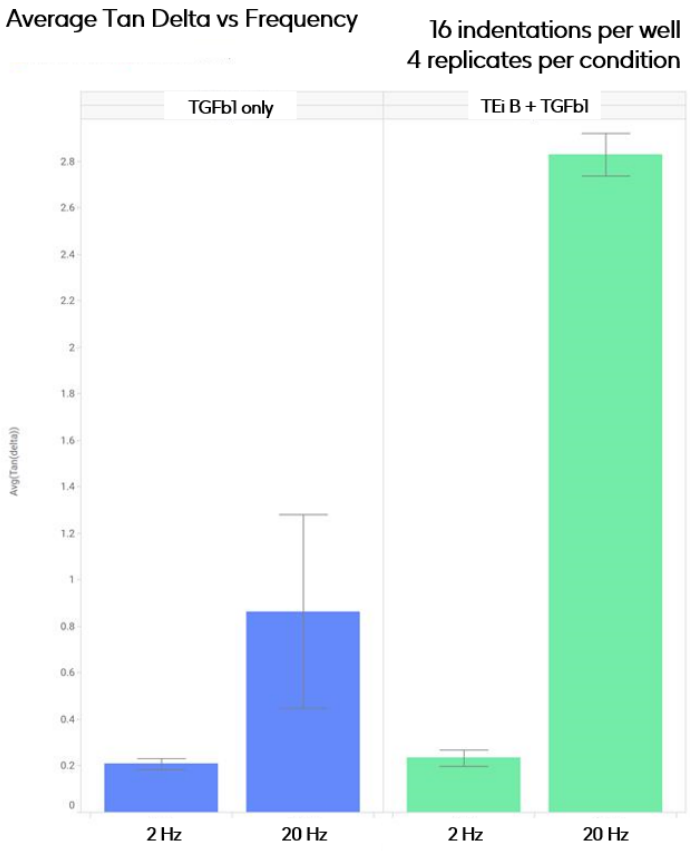

Figure 8: Figure 8. Bar plot of average tan δ values at 2 Hz and 20 Hz for TGF-β1-treated ECM with or without Target Enzyme inhibitor. *Bar plot showing mean tan δ values (±SEM) at 2 Hz and 20 Hz for each treatment group. Control samples not shown due to insufficient ECM yield. Data represents mean and Sd deviation, n=16 indentations per well, 4 wells per condition, n=1 donor.*

3.5 DMA: Repeat with Multiple Donors

To verify that the effects of the Target Enzyme inhibitor on ECM viscoelasticity were consistent across different patient samples, dynamic mechanical analysis was repeated using fibroblasts from three independent IPF donors (L279, L287, and L300). No significant differences in tan δ values were found between the TGF-β1-only and TGF-β1 plus inhibitor groups across all donors (figure 9A-B). Notably, control samples were excluded because the ECM was too thin and fragile to yield reliable indentation results.

Additionally, when data from all three donors were pooled (Figures 9 (C–D)), no statistically significant differences in the average tan δ were detected.

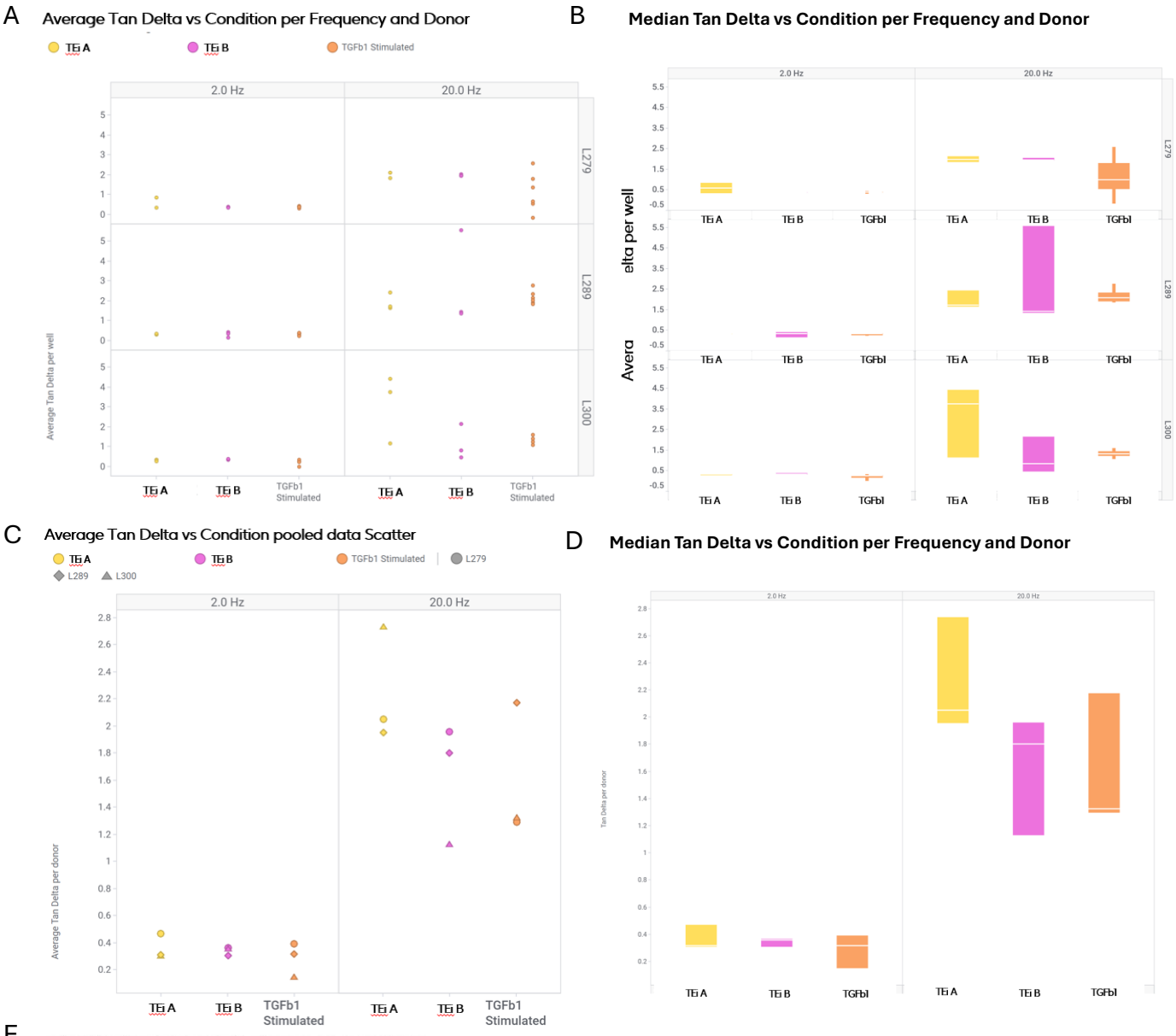

Figure 9. Scatter, box, and bar plots of tan δ values at 2 Hz and 20 Hz across donors and treatments. *(A–B) Scatter (mean) and box (median) plots of tan δ values at 2 Hz and 20 Hz, grouped by donor and treatment condition. (C–D) Scatter (mean) and box (median) plots of pooled tan δ values at 2 Hz and 20 Hz for each treatment group. Control samples not shown due to insufficient ECM yield. (E) Kruskal-Wallis fold change analysis results for fixed ECM pooled across conditions. Data represents mean, median, and Sd deviation, n=49 replicates per condition n=3 donor.*

Discussion

This study set out to explore how fibrotic stimuli, the Target Enzyme (TE), and its inhibition affect the mechanical and viscoelastic properties of extracellular matrix (ECM) produced by IPF fibroblasts. A 2D ECM model was used to assess relative stiffness and viscoelasticity under different treatment conditions, while also accounting for technical factors such as sample fixation and indentation depth.

The results showed that TGF-β1 stimulation led to increased ECM stiffness, but this was only clearly measurable at a deeper indentation depth (750 nm) and in methanol-fixed samples. Further analysis revealed that the probe only indents the surface of the ECM substrate when indenting at shallower indentation depths, explaining the inconclusive trend observed at 250 nm indentations. In unfixed or fragile ECM, the same effect wasn't detected highlighting limitations of measuring the stiffness of native 2D ECM and ECM formed in the absence of pro-fibrotic stimuli. TE alone also appeared to increase stiffness, and the effect was further enhanced when combined with TGF-β1.

Furthermore, treatment with TE inhibitors, particularly Inhibitor A, reduced ECM stiffness in fixed samples from multiple IPF donors. These results are consistent with Jones et al. (2018), who demonstrated in a long-term 3D in vitro IPF fibroblast model that dual LOXL2/3 inhibition, that works via a similar mechanism, normalized collagen architecture and significantly reduced ECM stiffness, supporting our observation that TE inhibitor A softens fixed fibrotic ECM [21]. However, this reduction in stiffness wasn't seen in unfixed ECM, again most likely due to the matrix being too thin and fragile to be accurately measured by the indentation probe.

The trend of unfixed ECM being unmeasurable was a consistent finding across most measurements. Methanol fixation was critical for generating reliable and repeatable data. Fixed samples were more likely to yield successful indentations and showed less variability, with data points clustering more closely around the mean. That said, fixation also introduces changes to the ECM that might reduce the biological accuracy of the model. The viscoelasticity results supported the observed stiffness findings in this study whereby for samples treated with TGF-β1, *tan δ* values were consistently lower across all the frequencies tested. This usually indicates more elastic, and therefore stiffer or fibrotic, ECM behaviour as seen in recent studies showing that lower *tan δ* under TGF- β1 exposure correlates with enhanced fibrotic differentiation and mechanotransduction[22]. On the other hand, samples that were treated with TE inhibitors tended to show higher *tan δ*, suggesting a shift toward more viscous and potentially less fibrotic properties. This pattern was quite clear in the earlier single-donor tests. However, when we repeated the analysis across three different IPF donors, the results were less consistent. No significant differences were observed, which probably reflects natural variation between donor samples. This points to the need for a larger cohort of donors to achieve significant results.

Another issue that was consistently observed across all experiments was the physical fragility of the unfixed ECM. This was especially a problem in control samples that had not been stimulated. Even in fibrotic conditions, the maximum indentation depth that could reliably be probed was around 5 µm. In control wells, the matrix was often vastly thinner, so deeper indentation was not possible. For these samples, a shallow indentation depth of approximately 250nm was required. As a result, direct comparisons between treatments were not always possible since we were not probing the same mechanical layers.

Another limitation of this study was that the flat 2D ECM setup doesn't reflect the complexity or structural integrity of fibrotic lung tissue[23], which puts into question the translational relevance of these results obtained.

Because of these limitations, we started to develop a 3D fibrosis model with the use of spheroids. This model brings several advantages compared to the flat 2D system, mainly more ECM build-up, better mechanical strength, and a microenvironment that's more accurate to what is seen in fibrotic tissue. Jones et al show that spheroids grown with fibroblasts from IPF patient tissue form dense regions of fibroblast foci also observed in human IPF lung tissue, suggesting that this model recapitulates at least some aspects of human lung fibrosis[24]. Thus, the second half of my project involved testing different spheroid culture platforms, including Kugelmeier and Corning Elplasia plates as shown in Figure 10 (A) and (B). Both of these support high-throughput spheroid generation due to containing multiple microwells per well, but they come with the caveat that the well V-bottom geometry makes them incompatible with the Pavone Nanoindenter. We also discovered from concordant experiments that seeding 25,000 cells per spheroid resulted in the optimum size required to comfortably indent spheroids and get accurate measurement of their mechanical properties. The microwells in these plates however had a maximum seeding density of 10,000-15,000 cells per microwell, therefore suitably sized spheroids could not be generated using these plates.

Thus, we moved to Akura 96-well plates as shown in Figure 10 (C) whereby we were able to seed more cells per well and produce larger spheroids suitable for nanoindentation by Pavone. That said, the narrow diameter of the microwells (around 1 mm) did not facilitate direct indentation of spheroids in these well plates. To allow indentation, spheroids can be transferred to collagen-coated 24-well flat-bottom plates before testing. To stop the spheroids from moving during indentation, simple but effective methods like drawing boundaries with hydrophobic barrier pens or scraping shallow safety zones with a scalpel and then embedding the spheroids in collagen can be used to keep them immobilised for measurement. These adjustments have made it much easier to carry out stable and accurate measurements of spheroids using the Pavone probe.

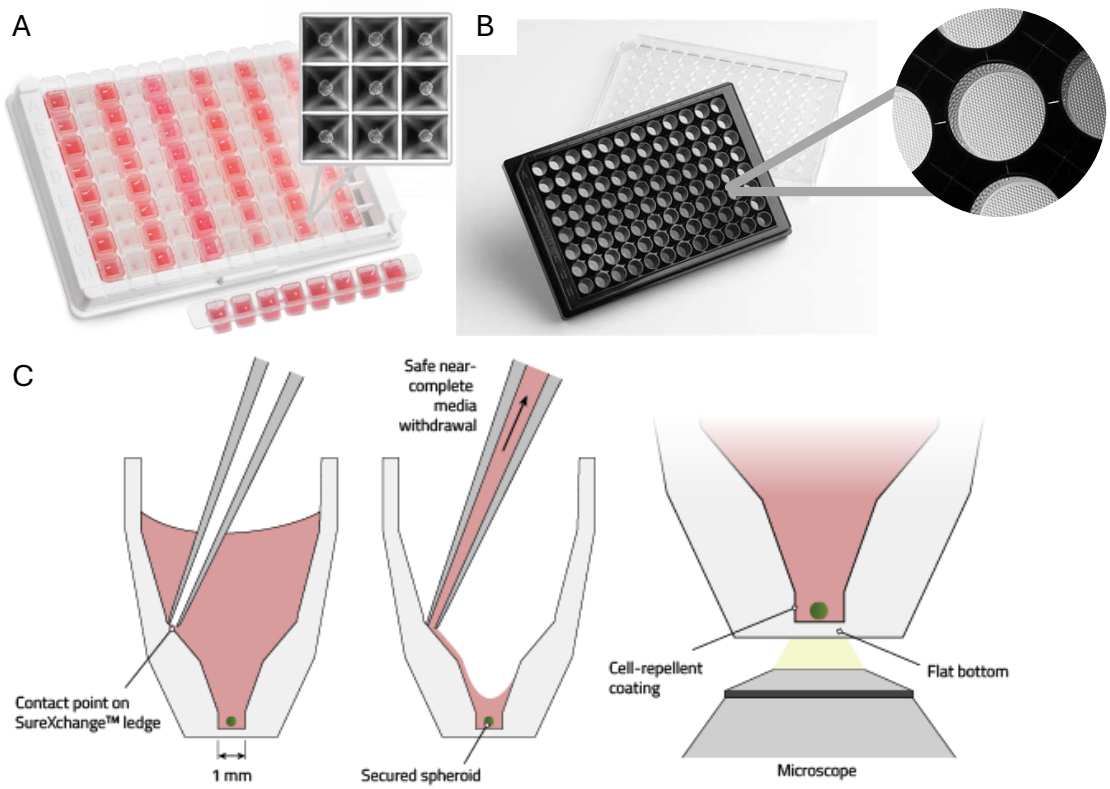

Figure 10: Comparison of 3D spheroid culture platforms for ECM studies. *(A) Kugelmeier 96-well plate and (B) Corning Elplasia plate, both designed for high-throughput spheroid formation but incompatible with mechanical indentation due to their V-bottom geometry. (C) Schematic of Akura 96-well plate microwell featuring a ~1 mm-wide cavity for consistent spheroid formation. While Akura plates support uniform spheroids, their small well diameter limits direct indentation, prompting transfer to flat-bottom plates for mechanical testing.*

In summary, the findings from both stiffness and viscoelasticity experiments point to quantifiable changes in ECM mechanics in response to TGF-β1, the Target Enzyme, and its inhibitors. The current 2D model however displayed some limitations, including technical challenges, and how translationally relevant it is to human tissue. Moving towards a 3D, spheroid-based ECM model could more accurately simulate in vivo fibrosis and mitigate some of the mechanical restrictions observed with the 2D model. This is an important finding in the context of IPF patients whereby lung stiffness is a hallmark of disease and correlates with declining lung function and poorer patient outcomes[24]. As current clinical tools to measure stiffness are indirect and limited, developing an in-vitro system that can quantitatively test anti-fibrotic therapy on mechanical properties of fibrosis offers a promising platform to assess the functional impact of anti-fibrotic therapies. By mimicking the biomechanical environment of an IPF diseased lung, these models could provide critical insights into how therapies influence tissue and, in the future, potentially guide the development of treatments that do more than slow fibrosis.

Over the course of my placement year, I worked on building and validating custom protocols for characterizing mechanical properties of ECM using the Pavone Nanoindenter. These included approaches for measuring both stiffness and viscoelasticity in 2D cultures and helped set the stage for more consistent, higher-throughput biomechanical testing. The project also promoted the transition from simple 2D models to advanced 3D systems, such as spheroids and potentially tissue or organoid platforms. Together, these steps lay the foundation for future fibrosis research at GSK, aiming to create

in vitro models that more accurately reflect patient disease to support the drug discovery of next generation anti-fibrotic therapies.

References

1. Sun, M., Spill, F., & Zaman, M.H. (2025). Single-cell transcriptome analysis revealing mechanotransduction via the Hippo/YAP pathway in promoting fibroblast-to-myofibroblast transition and idiopathic pulmonary fibrosis development. *ScienceDirect*. https://www.sciencedirect.com/science/article/pii/S0378111925000599
2. Optics11 Life. (n.d.). *Pavone Nanoindenter*. Retrieved from **HTTPS://WWW.OPTICS11LIFE.COM/PRODUCTS/PAVONE-NANOINDENTER/**
3. Asano, S., et al. (2024). In Vitro Modeling of Idiopathic Pulmonary Fibrosis: Lung-on-a-Chip and Hydrogel-Based Approaches. *International Journal of Molecular Sciences*, 25(21), 11751. https://www.mdpi.com/1422-0067/25/21/11751
4. Hoffman, T., et al. (2024). Pulmonary matrix-derived hydrogels from patients with idiopathic pulmonary fibrosis reveal differential fibroblast activation. *Molecular Biology of the Cell*, 35(8), mbc.E23-11-0428. https://www.molbiolcell.org/doi/pdf/10.1091/mbc.E23-11-0428
5. Chandar, V., Goykadosh, B.M., & Parameswaran, H. (2025). Intercellular contact is sufficient to drive Fibroblast to Myofibroblast transitions. *arXiv preprint*. https://arxiv.org/abs/2503.01834
6. Guo, T., et al. (2023). Regulators, functions, and mechanotransduction pathways of matrix stiffness in hepatic disease. *Frontiers in Physiology*, 14, 1098129. https://www.frontiersin.org/articles/10.3389/fphys.2023.1098129/full
7. Nizamoglu, R., et al. (2024). Multi-Step Extracellular Matrix Remodelling and Stiffening in the Progression of Idiopathic Pulmonary Fibrosis. *International Journal of Molecular Sciences*, 24(2), 1708. https://www.mdpi.com/1422-0067/24/2/1708
8. Liu, F., et al. (2024). Adiponectin suppresses stiffness-dependent, profibrotic activation of human lung fibroblasts. *American Journal of Physiology-Lung Cellular and Molecular Physiology*, 326(2), L123–L134. https://dzl.de/publication/10-1152-ajplung-00037-2024/
9. Kono, T., et al. (2024). Piezo2 Is a Key Mechanoreceptor in Lung Fibrosis that Drives Myofibroblast Differentiation. *The American Journal of Pathology*, 194(4), 567–578. https://www.sciencedirect.com/science/article/pii/S0002944025000288
10. University of New Hampshire. (2023). *Pavone Nanoindenter | University Instrumentation Center*. Retrieved from https://www.unh.edu/research/university-instrumentation-center/uic-affiliated-instruments/pavone-nanoindenter
11. Optics11 Life. (n.d.). *High-Throughput Mechanical Screening Platform*. Retrieved from https://shinningtech.com/pdf/Pavone-Brochure.pdf
12. Optics11 Life. (n.d.). *Pavone: A High-Throughput Mechanical Characterization Platform for Biomaterials in Various Wellplates*. Retrieved from https://www.researchgate.net/publication/344327839_PAVONE_a_high-throughput_mechanical_characterization_platform_for_biomaterials_in_various_wellplates
13. Optics11 Life. (n.d.). *Application Note: Mechanobiology of Fibrosis*. Retrieved from https://www.optics11life.com/wp-content/uploads/Application-note-Fibrosis-ANMOF202305v2.pdf
14. Liu, F., Lagares, D., Choi, K. M., Stopfer, L., Marinković, A., Vrbanac, V., … & Tschumperlin, D. J. (2015). *Mechanosignaling through YAP and TAZ drives fibroblast activation and fibrosis*. Journal of Clinical Investigation, **125**(3), 1069–1080. https://doi.org/10.1172/JCI74787

15. Parker, M. W., Rossi, D., Peterson, M., Smith, K., Sikström, K., White, E. S., … & Lagares, D. (2014). *Fibrotic extracellular matrix activates a profibrotic positive feedback loop*. Journal of Clinical Investigation, **124**(4), 1622–1635. https://doi.org/10.1172/JCI71386
16. Booth, A. J., Hadley, R., Cornett, A. M., Dreffs, A. A., Matthes, S. A., Tsui, J. L., … & White, E. S. (2012). *A cell–matrix model of fibrogenesis recapitulates characteristic features of idiopathic pulmonary fibrosis*. American Journal of Respiratory Cell and Molecular Biology, **46**(6), 825–834. https://doi.org/10.1165/rcmb.2011-0172OC
17. de Hilster, R. H. J., Sharma, P. K., Jonker, M. R., White, E. S., Gercama, E. A., Roobeek, M., … & Burgess, J. K. (2020). *Human lung extracellular matrix hydrogels resemble the stiffness and viscoelasticity of native lung tissue*. American Journal of Physiology-Lung Cellular and Molecular Physiology, **318**(4), L698–L704. https://doi.org/10.1152/ajplung.00360.2019
18. Perepelyuk, M., Chin, L., Cao, X., Van Sciver, R. E., Patel, V., & Sack, M. N. (2016). *Normal and fibrotic rat livers demonstrate shear strain softening and compression stiffening: a model for soft tissue mechanics*. PLoS ONE, **11**(1), e0146588. https://doi.org/10.1371/journal.pone.0146588
19. Georges, P. C., & Janmey, P. A. (2005). *Cell type–specific response to growth on soft materials*. Journal of Applied Physiology, **98**(4), 1547–1553. https://doi.org/10.1152/japplphysiol.01121.2004
20. Solon, J., Levental, I., Sengupta, K., Georges, P. C., & Janmey, P. A. (2007). *Fibroblast adaptation and stiffness matching to soft elastic substrates*. Biophysical Journal, **93**(12), 4453–4461. https://doi.org/10.1529/biophysj.106.101386
21. Mark G Jones et al (2018) Nanoscale dysregulation of collagen structure-function disrupts mechano-homeostasis and mediates pulmonary fibrosis eLife 7https://doi.org/10.7554/eLife.36354
22. Sacco, J. L., Vaneman, Z. T., & Gomez, E. W. (2024). Extracellular matrix viscoelasticity regulates TGFβ1-induced epithelial-mesenchymal transition and apoptosis via integrin linked kinase. *Journal of cellular physiology*, *239*(2), e31165. https://doi.org/10.1002/jcp.31165
23. Li, D., Zhang, X., Song, Z., Zhao, S., Huang, Y., Qian, W. and Cai, X. (2024), Advances in common *in vitro* cellular models of pulmonary fibrosis. Immunol Cell Biol, 102: 557-569. https://doi.org/10.1111/imcb.12756
24. Booth, A. J., Hadley, R., Cornett, A. M., Dreffs, A. A., Matthes, S. A., Tsui, J. L., Weiss, K., Horowitz, J. C., Fiore, V. F., Barker, T. H., Moore, B. B., Martinez, F. J., Niklason, L. E., & White, E. S. (2012). Acellular normal and fibrotic human lung matrices as a culture system for in vitro investigation. *American journal of respiratory and critical care medicine*, *186*(9), 866–876. https://doi.org/10.1164/rccm.201204-0754OC